




## Synchronized resistance of inhomogeneous magnetically induced dephasing of an image stored in a cold atomic ensemble

Ying-Hao Ye, Lei Zeng, Yi-Chen Yu, Ming-Xin Dong, En-Ze Li, Wei-Hang Zhang, Zong-Kai Liu, Li-Hua Zhang ,  
Guang-Can Guo, Dong-Sheng Ding \*, and Bao-Sen Shi †

*Key Laboratory of Quantum Information, University of Science and Technology of China, Hefei, Anhui 230026, China  
and Synergetic Innovation Center of Quantum Information and Quantum Physics, University of Science  
and Technology of China, Hefei, Anhui 230026, China*



(Received 23 January 2021; revised 6 May 2021; accepted 6 May 2021; published 19 May 2021)

Long-lived storage of arbitrary transverse multimodes is important for establishing a high-channel-capacity quantum network. Most of the pioneering works focused on atomic diffusion as the dominant impact on the retrieved pattern in an atom-based memory. In this work, we demonstrate that the unsynchronized Larmor precession of atoms in the inhomogeneous magnetic field dominates the distortion of the pattern stored in a cold-atom-based memory. We find that this distortion effect can be eliminated by applying a strong uniform polarization magnetic field. By mapping signal light into a spin wave between a pair of clock states, the destructive interference between different spin-wave components is diminished, and the stored localized patterns are synchronized further in a single spin-wave component; then, an obvious enhancement in preserving patterns for a long time is obtained. The reported results are promising for studying transverse multimode decoherence in optical storage and may find potential applications in the field of high-dimensional quantum networks in the future.

DOI: [10.1103/PhysRevA.103.053316](https://doi.org/10.1103/PhysRevA.103.053316)

### I. INTRODUCTION

As a robust carrier of information, a photon has many degrees of freedom, such as frequency, polarization, and transverse multimode [1,2], in which information can be encoded. Among them, the transverse multimode has received great attention because a transverse mode such as the Laguerre-Gaussian [3–6] can form an infinite-dimensional Hilbert space. By encoding information in a transverse multimode, one can dramatically increase the channel capacity of quantum information processing [7,8]. In the quantum information field, due to the long coherence time between metastable states of atoms, a long-lived quantum memory based on an atomic ensemble [9–11] could be achieved, which is promising for realizing quantum repeaters to overcome the strong attenuation of optical channels in a long-distance quantum network [12–20]. A quantum memory that is able to store quantum states for a long time can increase the success probability for entanglement creation per round-trip time and thereby decrease the time to establish entanglement between the end nodes in a quantum network [16]. Thus the study of long-lived storage of light with a spatial transverse multimode in atomic ensembles is increasingly in demand [2,8,21–26] for establishing a high-capacity quantum network.

A lot of significant works on storing a transverse multimode have been realized in a cold atomic ensemble [21,27,28]; however, none of these works focused

on prolonging the storage time, i.e., the achieved time for storing an image is only up to several microseconds. Although many works have achieved long-time storage in atomic ensembles [9–11], the stored field is still a single mode. Since the pioneering work of Pugatch [29] proved that optical modes with phase singularities are robust to strong diffusion of hot atoms in an atomic vapor, many elaborate schemes have been proposed to store the transverse multimode for a long time [30]. Techniques such as utilizing the diffraction property of the lens [31,32], employing a coupling light with a tailored transverse phase analogous to phase-shift lithography [33], or making use of the ghost imaging technique [34] are used to realize the image storage up to tens of microseconds. However, when we consider the transverse multimode storage in a cold atomic ensemble, the dominant deteriorating effect originated from atomic motion considered in previous works can be neglected due to the short storage time on the scale of microseconds, and therefore exploring the dephasing mechanism of storing a transverse multimode becomes significantly important.

Here we find that the inhomogeneous magnetically induced dephasing effect is the dominant source for the distortion of stored patterns. Usually, a complex pattern has more complicated spectrum distributions on the Fourier plane (FP) compared to the Gaussian mode; therefore, the spatial overlap between the diffracted pattern and ambient magnetic field is larger, and thus the stored pattern is more vulnerable to the unsynchronized evolution of the stored spectrum caused by the gradient of the magnetic field. In this work, we describe this distortion effect based on the dark state polaritons (DSPs) evolution theory [35,36]. According to the theory,

\*dds@ustc.edu.cn

†drshi@ustc.edu.cn

we propose a method to prolong the storage time of the transverse multimodes by applying a strong uniform polarization magnetic field that can synchronize the Larmor precession of atomic magnetic moments in different localized positions. We performed the experiment using a probe signal with two transversal patterns: snowflake shaped (six-fold rotational symmetric) and Greek alphabet  $\Psi$  shaped (axisymmetric). We achieved similar results for both patterns, and therefore the synchronization effect of a strong polarization magnetic field and the effect of state preparation in this article does not depend on the choice of a particular pattern. The experimental observations are in good agreement with the simulated results. To diminish destructive interference between different spin-wave components, we then initially prepare the atomic ensemble into  $|5S_{1/2}, F = 2, m_F = 0\rangle$ . When the polarization configuration of the signal light and coupling light is  $\text{lin} \perp \text{lin}$ , the signal light is mapped into spin waves between the clock states ( $|5S_{1/2}, F = 2, m_F = 0\rangle$  and  $|5S_{1/2}, F = 3, m_F = 0\rangle$ ) of the ground hyperfine levels of rubidium 85 (Rb85) [10,11]. Finally, by using the clock transition, the storage time of the transverse multimodes is prolonged by two orders of magnitude. Our method requires neither establishment of a sophisticated system to compensate for the inhomogeneous field [37] nor the use of a magnetic shield made of a high-permeability material [38].

## II. EXPERIMENTAL SETUP AND SIMULATION MODEL

The experiments were performed within the D1 transition of Rb85 as depicted in Fig. 1(a). We denote  $|5S_{1/2}, F = 2\rangle$ ,  $|5S_{1/2}, F = 3\rangle$  and  $|5P_{1/2}, F' = 3\rangle$  as  $|g\rangle$ ,  $|s\rangle$ , and  $|e\rangle$ , respectively. The coupling light is locked on the  $|s\rangle \leftrightarrow |e\rangle$  transition, and the center frequency of the signal field is resonant with the  $|g\rangle \leftrightarrow |e\rangle$  transition.

Our experimental arrangement is illustrated in Fig. 1(c). An atomic ensemble of Rb85 is trapped in a three-dimensional magneto-optical trap (MOT). Three pairs of mutually orthogonal Helmholtz coils are placed around the MOT to compensate for the static uniform magnetic field near the ensemble. Strong coupling light and weak signal light are input into the ensemble. To diminish decoherence from atomic motion, we let the signal light and coupling light propagate collinearly after PBS I to suppress the wave number of the spin wave. The coupling light and signal light are orthogonally circularly polarized and orthogonally linearly polarized with and without the quarter-wave plate (QWP in Fig. 1), respectively. The signal light passes through a pattern mask and the coupling light is focused by a lens with a focal length of  $f_3 = 300$  mm. The mask is placed at the front focal plane of the lens before the MOT with a focal length of  $f_1 = 500$  mm, and the spatial center of the MOT coincides with the back focal plane. After passing through lens  $f_1$ , the coupling light is shaped as a Gaussian beam with a waist diameter of 4.2 mm. In the paraxial approximation (the diameter of signal light is much smaller than the diameter of the lens in our experiment), a thin lens can approximately transform the pattern in the front focal plane to its Fourier spectrum in the back focal plane. This can be proven by substituting the phase transformation function of the thin lens in the paraxial approx-

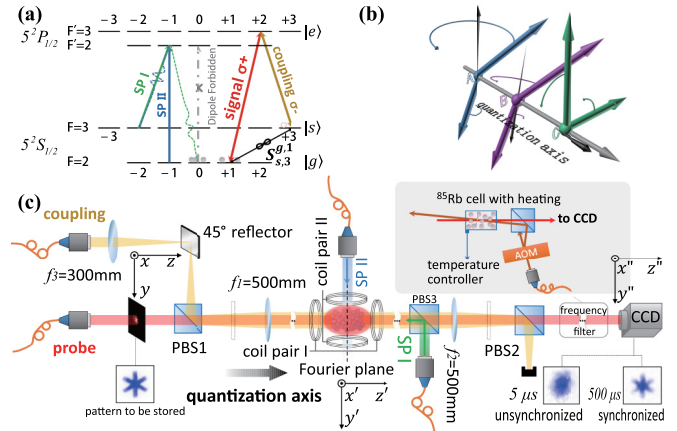


FIG. 1. (a) The corresponding energy levels. When signal light and coupling light are orthogonally circularly polarized, there exist four groups of spin waves in an unpolarized ensemble. After state preparation (SP), only one group of spin waves dominates. (b) The schematic of Larmor precession of atomic magnetic moments. The precession behavior of two initially identical spin waves is quite different in inhomogeneous magnetic fields, leading to different phases and intensities of DSPs after precession. At point C, when the polarized magnetic field is parallel with the quantization axis, the direction of the atomic magnetic momentum is perpendicular to the quantization axis, and therefore the DSPs undergoes the same evolution during precession. (c) Experimental setup. PBS: polarization beam splitter; QWP: quarter-wave plate; AOM: acoustic-optical modulator; CCD: ICCD camera.

imation,  $\exp[-ik(x^2 + y^2)/(2f)]$ , in the Fresnel diffraction formula [39] (where  $k$  is the wave vector and  $f$  is the focal length). Therefore, lens  $f_1$  works as a Fourier transformer for the signal light and produces Fraunhofer diffraction of the pattern on the mask at the FP [39]. For arbitrary patterns on the mask, the diffracted patterns in the atomic ensemble are robust to atomic diffusion due to the phase flipping between adjacent bright and dark spots [29,31,32]. Because the front focal plane of the lens after the MOT  $f_2 = 500$  mm coincides with the back focal plane of the lens  $f_1$ , the lens  $f_2$  and the lens  $f_1$  form a  $4f$  imaging system for the signal light, and thus the pattern of the mask is imaged on the ICCD (1024 by 1024, iStar 334T series, Andor).

To diminish the decoherence of DSPs originated from the ambient magnetic field, we prepare the initial states as  $|g, m_F = 0\rangle$ . This state preparation (SP) process uses a two-frequency optical pumping setup [40,41]. The relative energy levels are shown in Fig. 1(a). By illuminating the ensemble with  $\pi$  light [SP II in Fig. 1(a)] that is resonant with the  $|F = 2\rangle \leftrightarrow |F' = 2\rangle$  transition and linearly polarized light [SP I in Fig. 1(a)] that is resonant with the  $|F = 3\rangle \leftrightarrow |F' = 2\rangle$  transition propagating along the quantization axis simultaneously, the population of atoms in  $|g, m_F = 0\rangle$  in the ensemble accumulates because the optical transition  $|g, m_F = 0\rangle \rightarrow |5P_{1/2}, F' = 2, m_{F'} = 0\rangle$  is electric dipole forbidden (see Table 19 in Ref. [42]); after a period of time, the majority of the atoms (approximately 70%) are in the desired state. The advantage of this two-frequency optical pumping method is that it does not require the creation of a population difference between different Zeeman sublevels or hyperfine states. The

polarization magnetic field should be large enough to split the electromagnetically induced transparency (EIT) transmission peak [43]; after SP, only one transmission peak dominates.

Although PBS2, PBS3, and the Glan-Taylor prism in Fig. 1 work as polarization filters for orthogonally polarized signal and coupling light, a more delicate filter is needed to filter the strong coupling light out when the signal light and coupling light are propagating collinearly. The traditional Fabry-Pérot etalon is not suitable because not every transverse multimode can survive in the optical cavity. Therefore, we use the Rb85 absorption cell as a narrow bandpass filter. As shown in the inset of Fig. 1(c), an expanded pump light passes through the absorption cell in a direction nearly opposite to that of the signal light. Our experiment runs periodically with a repetition rate of 50 Hz. In each cycle, the cooling light is turned off 500  $\mu$ s before the repump light is turned off so that all the atoms can be prepared in the  $|g\rangle$  state. The polarization coil is turned on 60  $\mu$ s before the MOT starts to be turned off to establish the SP magnetic field. The experimental window opens 300  $\mu$ s after the MOT starts to be turned off. Before the experimental window opens, two SP light beams are turned on for 50  $\mu$ s. The exposure time of the ICCD is set to 100 ns, which matches the width of the retrieved pulse, and every captured retrieved image presented in this article is the average result of 1000 captures.

We place two pairs of coils around the MOT [see Fig. 1(c)]. Coil pair I, which is parallel to the signal light, can generate a strong uniform polarization magnetic field in the vicinity of the ensemble and works as polarized coils. In the experiment, the applied inhomogeneous magnetic field is from a pair of anti-Helmholtz coils (coil pair II). To probe the inhomogeneous magnetic field generated by coil pair II, we use another coil pair III [not shown in Fig. 1(c)] as probe coils, which has an inductance much smaller than that of the polarized coils and coil pair II and is perpendicular to coil pair I. By observing the voltage across the probe coils during the experiment, we can detect and estimate the inhomogeneous magnetic field. We ignore the mutual inductance between the probe coils and other coils; thus, the rate of change in the inhomogeneous magnetic field strength in the vicinity of the ensemble can be estimated by  $d\vec{B}(t)/dt \approx -\chi U(t)/(NS)$ . Here,  $N$  and  $S$  are the number of turns and the cross-sectional area of the probe coils, respectively. The coefficient  $\chi$  is the ratio of the average intensities of the magnetic field near the ensemble and the probe coils, which is calculated to be 0.024 in our experiment. The change in the inhomogeneous magnetic field during 20  $\mu$ s of storage is estimated to be of the order of  $O(\sim 1 \times 10^{-4}$  G), which is much smaller than its initial strength; therefore, this inhomogeneous magnetic field can be seen as static during the simulation.

When the frequency of the signal light is scanned by an AOM, an EIT window appears at the two-photon resonance  $\omega_s - \omega_c = \omega_{sg}$  [44], where  $\omega_s$  and  $\omega_c$  are the frequencies of the signal and coupling light, respectively, and  $\omega_{sg}$  is the energy difference between  $|s\rangle$  and  $|g\rangle$ . We imprint a signal pulse that is resonant with the  $|g\rangle \leftrightarrow |e\rangle$  transition onto the atomic ensemble, and then, this light pulse is transformed into DSPs [45,46]. By adiabatically turning off the coupling light, the group velocity of the DSPs decreases to zero and the photon components of the DSPs are mapped into collec-

tive Raman coherences between  $|s\rangle$  and  $|g\rangle$  [47]. The Raman coherence can be seen as spin waves, and we denote the spin wave between  $|g, m_1\rangle$  and  $|s, m_2\rangle$  as  $S_{s,m_2}^{g,m_1}$ . When the signal light and coupling light are orthogonally circularly polarized, four groups of spin waves exist. As illustrated in Fig. 1(b), the magnetic moments of atoms in  $|g, m_1\rangle$  and  $|s, m_2\rangle$  precess around the magnetic field; hence, the phase and population of different groups of spin waves change, which results in the collapse and revival of DSPs and then causes enhancement and reduction of the retrieval efficiency over the storage time. Because the beam waist of the expanded Gaussian coupling light is large compared to the diameter of the input pattern ( $\sim 1.6$  mm), we approximate it as a uniform plane wave hereafter. Therefore, both the intensity and phase information of the signal field in the FP are continuously converted into the spin wave,  $\sigma_{gs} = -gE/\Omega_c(t)$ , where  $E$  is the signal field and  $\Omega_c(t)$  is the Rabi frequency of the coupling light [45].

To simplify the theoretical analysis, we treat both the signal field and coupling light as monochromatic fields and assume that atoms are initially unpolarized. The temperature of the ensemble is measured to be approximately 200  $\mu$ K in a time-of-flight experiment, and therefore the most probable distance of thermal motion is calculated to be approximately 35  $\mu$ m after 20  $\mu$ s of storage. The optical depth and diameter of the rubidium ensemble is measured to be 5 mm for the signal light and around 2 mm, respectively; therefore, the mean free path is calculated to be of the order of  $O(\sim 10^2$  m), which is much larger than the ensemble, and thus the atomic collision can be neglected in this article. In addition to the thermal motion, a neutral atom with a magnetic moment experiences a force in the gradient magnetic field. When the ambient electric field can be neglected, the neutral atom motion can be calculated as  $\dot{p} = -(\mu_F \cdot \nabla)B(r)$ . The gradient of the magnetic field,  $\partial_{x_i} B_j$ , is measured to be of the order of  $O(\sim 1$  G/m), and thus, the acceleration of an individual atom is of the order of  $O(\sim 10^{-2}$  m s $^{-2}$ ). During a short storage time (tens of microseconds), the extra drift displacement originating from the magnetic gradient is of the order of  $O(\sim 10^{-3}$  nm), which is much smaller than that of the atom thermal motion. Therefore, treating atoms as motionless particles in the simulation when the storage time is relatively short ( $< 20$   $\mu$ s) is reasonable since the average motion is much smaller than the size of the Fraunhofer diffraction pattern stored in the ensemble.

We establish the Cartesian coordinate system shown in Figs. 1(c) and 2, in which the quantization axis  $z$  is parallel to the propagation direction of the signal field. The signal light propagates as DSPs after entering the atomic ensemble, and the annihilation operator of the DSPs has the following form [35]:

$$\hat{\Psi}(x', y', z, t) = \frac{i\Omega(t)\hat{a}_\alpha - \sqrt{Np}\kappa^* \sum_m R_m(\alpha, \beta) \hat{S}_{s,m+\alpha-\beta}^{g,m}}{\sqrt{\Omega^2 + Np|\kappa|^2 \sum_m R_m^2(\alpha, \beta)}}, \quad (1)$$

where  $\alpha$  and  $\beta$  are the helicities of the polarization of the signal light and coupling light, respectively,  $\hat{a}_\alpha$  is the annihilation operator of the signal photon,  $N$  is the number of atoms in the ensemble,  $\kappa$  is the coupling constant for the signal transition,  $p = 1/(2F_g + 1)$ , and the real

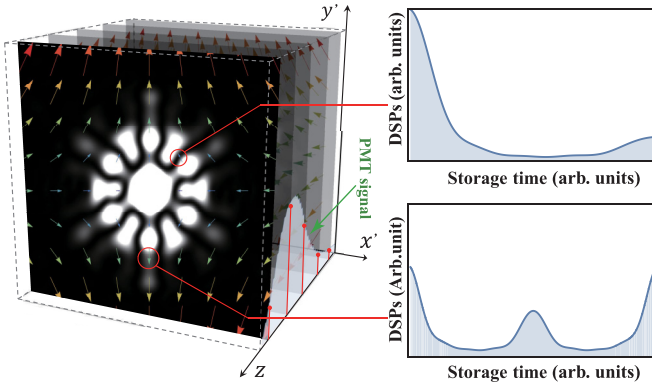


FIG. 2. The localized inhomogeneous magnetic field at different positions leads to different evolution behaviors of spin waves; thus, the deformation of the intensity and phase distribution of DSPs with time can be calculated. We use the weighted average of the data along the  $z$  axis as the simulation result.

coefficient  $R_m(\alpha, \beta) = C_{m, \alpha, m+\alpha}^{F_g, 1, F_e} / C_{m+\alpha-\beta, \beta, m+\alpha}^{F_s, 1, F_e}$  is determined by Clebsch-Gordan (CG) coefficients related to the spin waves. After the coupling light is adiabatically turned off, the photonic components of the DSPs transform into spin-wave components, and then, the annihilation operator of the DSPs has the following form:

$$\begin{aligned} \hat{\Psi}(x', y', z, t_s = 0) & \\ & \propto \sum_m R_m(\alpha, \beta) \Gamma(x', y', z) \hat{S}_{s, m+\alpha-\beta}^{g, m}(x', y', z, t_s = 0) \\ & \propto \sqrt{P(z)} \sum_m R_m(\alpha, \beta) \Gamma(x', y', z) u_f(x', y', t_s = 0), \quad (2) \end{aligned}$$

where  $u_f(x', y', t_s = 0)$  is the amplitude of the signal light in the FP before storage.  $P(z)$  is a phenomenological coefficient that describes the weight of the spin wave at different  $z$  and satisfies  $\int_{-\infty}^{+\infty} P(z) dz = 1$ .  $\Gamma(x', y', z)$  is the distribution function taking into account the spatial variation of the atomic ensemble density. For a spherical-shaped atomic ensemble with a Gaussian density distribution, we have  $\Gamma(x', y', z) \propto \exp[-(x'^2 + y'^2 + z^2)/\sigma^2]$ , where  $\sigma$  is the measured radius of the atomic ensemble, and  $u_f$  can be calculated by

$$u_f(x', y', t_s = 0) \propto \frac{1}{i\lambda f_1} \exp\left[-i\frac{2\pi}{\lambda f_1}(x'x + y'y)\right] dx dy, \quad (3)$$

where  $u_o$  is the amplitude of the signal field in the object plane of the  $4f$  system and is proportional to the square root of the intensity information recorded by the ICCD. We assume that  $u_o$  has a uniform phase distribution because the pattern mask is illuminated by collimated signal light. The evolution of the retrieved signal with time depends on both the intensity and orientation of the ambient magnetic field with respect to the signal vector. Therefore, the evolution of DSPs at different points in the transverse plane is different due to the gradient of the inhomogeneous magnetic field. By substituting Eq. (2) in Eq. (1), letting  $\Omega = 0$ , and applying the rotation operator to the relevant magnetic substates of the stored coherence using

the theory in Refs. [35,36], we have

$$\begin{aligned} \hat{\Psi}(x', y', z, t_s = t) & \\ & \propto \sqrt{P(z)} \sum_{m'} \sum_m R_{m'} R_m [D_{m', m}^g]^\dagger D_{m'+\alpha-\beta, m+\alpha-\beta}^s \\ & \quad \times \Gamma(x', y', z) u_f(x', y', t_s = 0). \quad (4) \end{aligned}$$

The DSPs at  $t_s = t$  are determined by the spin waves at that moment, and the spin wave at  $t_s = t$  can be calculated by applying a quantum rotation operator on the Zeeman sublevels of the spin wave at  $t_s = 0$ ; the latter is in proportion to the amplitude of the signal light. The evolution difference between DSPs at different points in the gradient magnetic field results in deformation of the intensity and phase information in the FP and thus leads to downgrading of the similarity. In a stationary ambient magnetic field  $\partial_t B = 0$ , the matrix element of the rotation operator between different quantized levels of hyperfine level  $F$  is  $D_{m', m}^F(x', y', z, t) = \langle F, m' | \exp[-ig_F \mu_B B(x', y', z) \cdot \hat{F} t / \hbar] | F, m \rangle$ , where  $\hat{F}$  is the total angular momentum operator,  $g_F$  is the Landé  $g$  factor of hyperfine level  $F$ , and  $\mu_B$  is the Bohr magneton. The quantization axis is chosen to be parallel to the signal field direction. The retrieved signal field intensity is proportional to the number of DSPs. After the second coupling pulse illuminates the ensemble, we have the retrieved signal  $|u_f(x', y', t_s = 0)|^2 = \langle \hat{\Psi}^\dagger \hat{\Psi} \rangle$ . We denote the calculated relative retrieval efficiency at each transverse point by  $\eta$  and the corresponding additional phase angle at that point by  $\phi$ ; taking the quasibosonic property of the spin wave into consideration,

$$\begin{aligned} \eta & \propto |\Gamma|^2 \left| \sum_{m', m} R_{m'} R_m [D_{m', m}^g]^\dagger D_{m'+\alpha-\beta, m+\alpha-\beta}^s \right|^2, \\ \phi & = \text{Arg} \left( \sum_{m', m} R_{m'} R_m [D_{m', m}^g]^\dagger D_{m'+\alpha-\beta, m+\alpha-\beta}^s \right). \quad (5) \end{aligned}$$

Because  $P(z)$  satisfies the normalization condition, the retrieved pattern has the following form:

$$\begin{aligned} I(x'', y'', t_s = t) & \\ & \propto \int_{-r_a/2}^{r_a/2} dz P(z) \mathcal{F}[e^{-i\phi} \sqrt{\eta} u_f(x', y', t_s = 0)], \quad (6) \end{aligned}$$

where  $\mathcal{F}[\cdot]$  denotes the Fourier transformation of the lens  $f_2$ . To numerically simulate the retrieved signal, we need to sample Eq. (6). Because  $P(z)$  does not have a singular point, the normalization property can be approximated as  $\sum_{z'=-R}^R P(z') \delta z' = 1$ , where  $R$  is the radius of the atomic ensemble, and we have

$$I(x'', y'', t_s = t) \propto \sum_{z'} P(z') \mathcal{F}[e^{-i\phi} \sqrt{\eta} u_f(x', y', t_s = 0)] \delta z'. \quad (7)$$

The similarity between the retrieved and original images is quantitatively defined by  $S = \sum_{m, n} A_{mn} B_{mn} / \sqrt{\sum_{m_1, n_1} A_{m_1, n_1}^2 \sum_{m_2, n_2} B_{m_2, n_2}^2}$ , where  $A_{mn}$  and  $B_{mn}$  are the intensities of the pixel in the  $m_{th}$  and  $n_{th}$  column of the retrieved and original images, respectively [48,49]. Taking the background into consideration, we define the relative similarity as  $S_r = (S - S_{bg}) / (1 - S_{bg})$ , where  $S_{bg}$  is the similarity between the original pattern and the background.

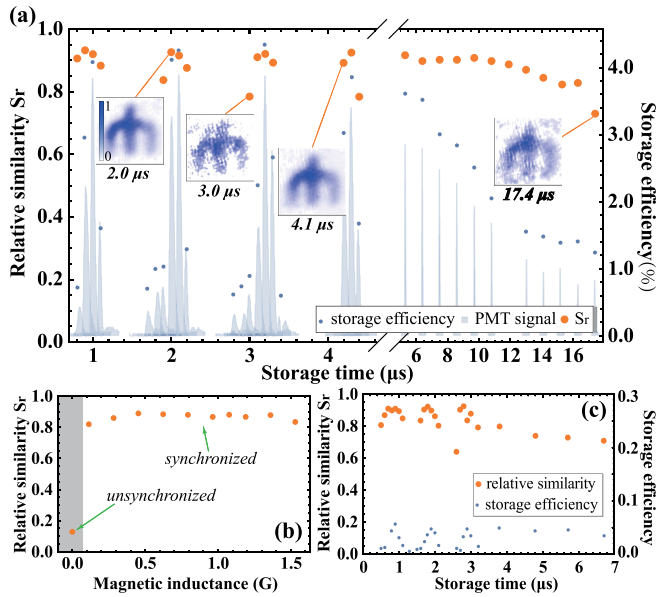


FIG. 3. (a) Evolution of DSPs and relative similarity with storage time. A static uniform polarization magnetic field ( $B_p \approx 0.97$  G) much larger than the inhomogeneous magnetic field ( $B_i \approx 0.05$  G) and parallel to the quantization axis is applied, and Larmor precession appears while the pattern of the retrieved signal remains. (b) When keeping the storage time unchanged ( $t_s = 6 \mu\text{s}$ ) and increasing the strength of the polarization magnetic field, as long as the magnetic field is strong enough to synchronize the atomic magnetic moments, the relative similarity increases dramatically. (c) When the direction of the polarization magnetic field is chosen to be perpendicular to the quantization axis, a similar result as in (a) can be achieved.

We use  $S_r$  in this work because it approaches zero when the pattern is completely smeared out.

### III. EXPERIMENTAL RESULT AND SIMULATION RESULT

From the theory, we find that the gradient of the inhomogeneous magnetic field, instead of the magnetic field itself, causes the deformation of the stored pattern. When a uniform polarization magnetic field much stronger than the inhomogeneous magnetic field is applied (the strength of the polarization field is shown in Fig. 3), the total ambient field in the vicinity of the ensemble can be seen as a uniform field in the transverse plane,  $\partial_x B_j$ , and hence, the precession of atomic magnetic moments is synchronized. Therefore,  $\eta$  and  $\phi$  are also uniform in the transverse plane. Although the destructive interference of different spin-wave components cannot be eliminated in this situation, the transverse distribution of the DSPs in the ensemble is preserved. As shown in Fig. 3(a), the pattern configuration remains even when the retrieval efficiency is very low, while the intensity of the retrieved signal shows Larmor precession. This synchronization effect can dramatically increase the relative similarity of the retrieved pattern [see Fig. 3(b)]. According to the theory, the polarization magnetic field is not necessarily parallel to the quantization axis. We achieved similar results by applying a polarization magnetic field perpendicular to the quantization axis [see Fig. 3(c)].

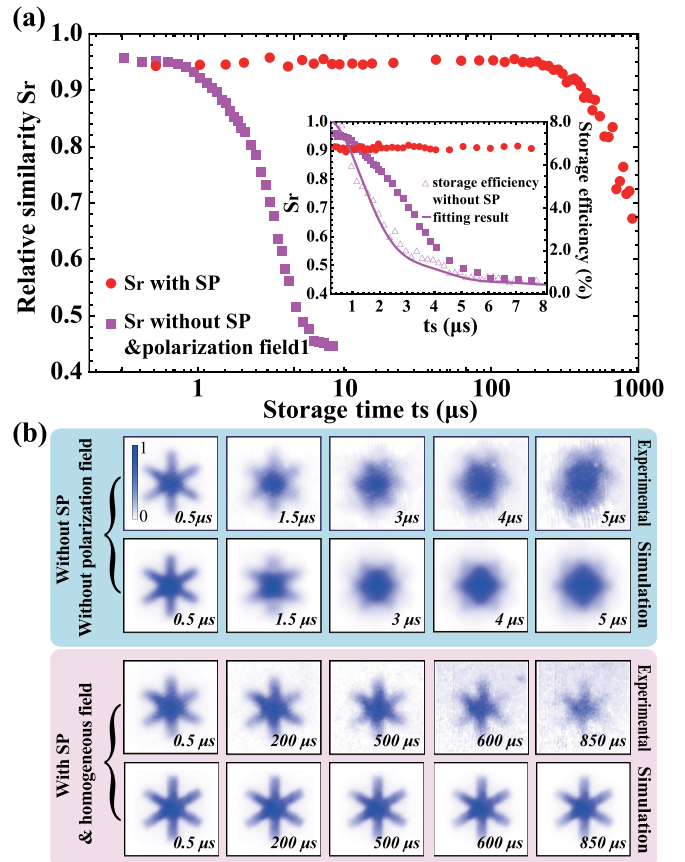


FIG. 4. (a) Relative similarity and storage efficiency as a function of storage time with SP and without SP. The storage time of the pattern is extended by two orders of magnitude after SP. The inset shows the decay of  $S_r$  and storage efficiency during a short storage time; the solid magenta line is the fitting result; and the fitting parameters are utilized in the simulation. (b) Retrieved pattern recorded by the ICCD and corresponding simulation results with and without SP. The pattern could be preserved for up to  $800 \mu\text{s}$  after SP. The simulation result in the last row has taken atomic diffusion into consideration.

In contrast to the former case, when the homogeneous polarization magnetic field is switched off, the retrieved pattern is dramatically blurred, as shown in Fig. 4. Because the motion of atoms can be neglected and the static uniform magnetic field has been compensated, this deformation phenomenon mainly originates from the inhomogeneous magnetic field. It is worth pointing out that the same technique can be used with thermal atomic vapors, despite the Doppler broadening being orders of magnitude larger, by adding a magnetic field of the order of a fraction of one Tesla. In the pioneering work of Whiting *et al.* [50], the addition of a magnetic field allows for exquisite control of the collective beat phenomenon of heralded signal photons from a collective spin excitation.

To achieve long-lived storage for arbitrary transverse multimodes, one needs to eliminate the decoherence of the DSPs. Here, we use SP process (see Fig. 1 and Sec. II) to prepare the majority of atoms in the ensemble into  $|g, m_F = 0\rangle$ . When the signal light and coupling light are tailored to be orthogonally linearly polarized, only one group of spin waves

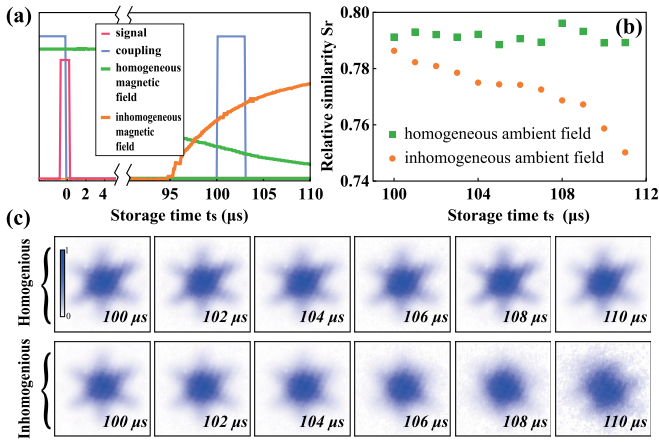


FIG. 5. (a) Time sequence of the experiment. (b) Relative similarity as a function of storage time with and without an inhomogeneous ambient magnetic field. The inhomogeneous magnetic field is applied at  $t_s = 95 \mu\text{s}$ . (c) Retrieved pattern recorded by the CCD.

$S_{s,0}^{g,0}$  dominates. Hence, the destructive interference among different groups of spin waves is diminished; and therefore the decoherence of the DSPs is dramatically reduced. Moreover, because the polarization magnetic field is chosen to be parallel to the quantization axis, we have  $D_{m,0}^F = \delta_{m,0}$  for arbitrary hyperfine level  $F$  and quantized sublevel  $m$ ; therefore, only an overall phase factor is picked up in the transverse plane during the precession, and the retrieved pattern remains unchanged. The above process can be schematically illustrated in an intuitive picture, depicted as case C in Fig. 1(b): all the atomic magnetic moments are perpendicular to the quantization axis, and the projection of the atomic magnetic moment on the quantization axis remains zero during the precession. The experimental result of the relative similarity as a function of storage time is plotted in Fig. 4(a) and the retrieval efficiency is also shown. The solid magenta line is the fitting result of the retrieval efficiency, and the fitting parameter is used as the strength of the inhomogeneous magnetic field. In the simulation of Fig. 4(b), we achieve an obvious prolongation of pattern preservation with time after SP. In the third row, the spatial information of the pattern is preserved for up to  $800 \mu\text{s}$  after SP, which is prolonged by two orders of magnitude compared to the first row, where the retrieved pattern is dramatically blurred after  $2 \mu\text{s}$  of storage. The simulation results shown in the second and fourth rows agree with the experimental results in the first and third rows. The atomic motion cannot be neglected for longer storage time (over one-hundred microseconds); for instance, the most probable distance of thermal motion exceeds  $10^2 \mu\text{m}$  after  $800 \mu\text{s}$  of storage. We have taken atomic diffusion into consideration for the simulation results in the fourth row using the theory proposed in Refs. [31,33].

In order to illustrate that the deformation of the retrieved pattern is dominated by the inhomogeneous magnetic field, we turn off the homogeneous polarization field after the spin waves are established, and the majority of spin waves are in  $S_{s,0}^{g,0}$ ; see the time sequence shown in Fig. 5(a). After  $95 \mu\text{s}$  of storage, we turn on a small inhomogeneous magnetic field,

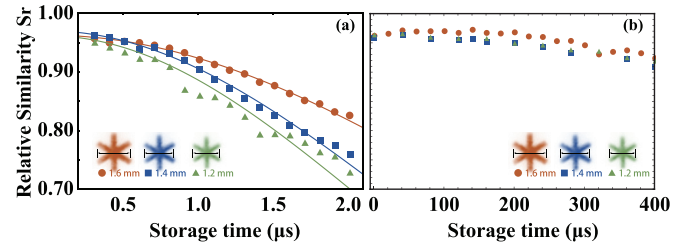


FIG. 6. Relative similarity as a function of time for patterns of different sizes. (a) Without SP and without strong polarization magnetic field. (b) With SP and strong polarization magnetic field.

and the average intensity of this field is calculated to be of the order of  $O(\sim 1 \times 10^{-2} \text{ G})$ , which is large enough to change the configuration of the existing residual homogeneous polarization field [the average intensity is calculated to be of the order of  $O(\sim 1 \times 10^{-2} \text{ G})$ ]. We found that even though the majority of spin waves are initially in  $S_{s,0}^{g,0}$  after the SP process (the SP efficiency is measured to be approximately 70% in an independent experiment), the unsynchronized precession of atomic magnetic moments in the inhomogeneous ambient magnetic field still leads to deformation of the retrieved pattern. The relative similarity as a function of storage time is shown in Fig. 5(b).  $S_r$  obviously decays faster in an inhomogeneous field. The corresponding CCD signal is shown in Fig. 5(c). The retrieved pattern remains nearly unchanged in a homogeneous ambient field, while the transverse information is smeared out after the inhomogeneous ambient field is turned on for  $10 \mu\text{s}$ .

In order to study the dependence of the  $S_r$  on the size of the pattern, we store the same pattern with three different sizes, and the experimental results are shown in Fig. 6. As the pattern size decreases, the overlap between diffracted patterns in the FP and the inhomogeneous magnetic field increases; therefore, the distortion effect of the inhomogeneous magnetic field on the stored pattern becomes more apparent, as shown in Fig. 6(a). In comparison with the former case, the difference between the decay rates of the  $S_r$  of different-size patterns decreases after SP because the deteriorating effect of the inhomogeneous magnetic field has been diminished; see Fig. 6(b).

#### IV. CONCLUSION

In conclusion, we theoretically and experimentally demonstrate that the inhomogeneous magnetic field is the main distortion effect on the stored image. The stored transverse multimode with a wider spatial frequency distribution in the FP is more vulnerable to the deformation effect because it has a larger overlap with the inhomogeneous magnetic field. The simulation results based on the model show good agreement with the experimental data. According to the model, we propose and demonstrate that a uniform polarization magnetic field can eliminate this deformation effect by synchronizing the Larmor precession. Additionally, we illustrate that by filtering out only one group of spin waves that address the clock transition [10,11], the decoherence of the DSPs and dephasing of the stored transverse multimode can be diminished, and the storage time is prolonged by two orders of magnitude.

The approach we propose demands neither a passive magnetic shield made of a high-permeability soft magnetic material nor an active compensation method that requires fast detection of the ambient magnetic field in a MOT. Recently, an important alternative method for protection of a collective state from inhomogeneous dephasing has been proposed by Finkelstein *et al.* [51]. Our work may benefit future research on the long-lived storage of transverse multimodes using technologies such as dipole trapping or dynamic decoupling [52,53] and has potential applications in quantum networks.

## ACKNOWLEDGMENTS

We acknowledge funding from the National Key R&D Program of China (Grant No. 2017YFA0304800), National Natural Science Foundation of China (Grants No. U20A20218, No. 61525504, No. 61722510, No. 61435011, and No. 11934013), Anhui Initiative in Quantum Information Technologies (Grant No. AHY020200), and the Youth Innovation Promotion Association of Chinese Academy of Sciences under Grant No. 2018490.

- 
- [1] J. H. Shapiro and R. W. Boyd, *Quantum Inf. Proc.* **11**, 949 (2012).
- [2] W. Zhang, D.-S. Ding, M.-X. Dong, S. Shi, K. Wang, S.-L. Liu, Y. Li, Z.-Y. Zhou, B.-S. Shi, and G.-C. Guo, *Nat. Commun.* **7**, 13514 (2016).
- [3] A. Mair, A. Vaziri, G. Weihs, and A. Zeilinger, *Nature (London)* **412**, 313 (2001).
- [4] G. Molina-Terriza, J. P. Torres, and L. Torner, *Nat. Phys.* **3**, 305 (2007).
- [5] M. Krenn, M. Malik, M. Erhard, and A. Zeilinger, *Philos. Trans. R. Soc. London A* **375**, 20150442 (2017).
- [6] K.-P. Marzlin, W. Zhang, and E. M. Wright, *Phys. Rev. Lett.* **79**, 4728 (1997).
- [7] A. Grodecka-Grad, E. Zeuthen, and A. S. Sørensen, *Phys. Rev. Lett.* **109**, 133601 (2012).
- [8] D.-S. Ding, W. Zhang, S. Shi, Z.-Y. Zhou, Y. Li, B.-S. Shi, and G.-C. Guo, *Light: Sci. Appl.* **5**, e16157 (2016).
- [9] B. Zhao, Y.-A. Chen, X.-H. Bao, T. Strassel, C.-S. Chuu, X.-M. Jin, J. Schmiedmayer, Z.-S. Yuan, S. Chen, and J.-W. Pan, *Nat. Phys.* **5**, 95 (2009).
- [10] R. Zhao, Y. Dudin, S. Jenkins, C. Campbell, D. Matsukevich, T. Kennedy, and A. Kuzmich, *Nat. Phys.* **5**, 100 (2009).
- [11] Y. Dudin, L. Li, and A. Kuzmich, *Phys. Rev. A* **87**, 031801(R) (2013).
- [12] L.-M. Duan, M. D. Lukin, J. I. Cirac, and P. Zoller, *Nature (London)* **414**, 413 (2001).
- [13] H.-J. Briegel, W. Dür, J. I. Cirac, and P. Zoller, *Phys. Rev. Lett.* **81**, 5932 (1998).
- [14] L. Jiang, J. M. Taylor, and M. D. Lukin, *Phys. Rev. A* **76**, 012301 (2007).
- [15] N. Sangouard, C. Simon, B. Zhao, Y.-A. Chen, H. de Riedmatten, J.-W. Pan, and N. Gisin, *Phys. Rev. A* **77**, 062301 (2008).
- [16] F. Bussi eres, N. Sangouard, M. Afzelius, H. De Riedmatten, C. Simon, and W. Tittel, *J. Mod. Opt.* **60**, 1519 (2013).
- [17] K. Heshami, D. G. England, P. C. Humphreys, P. J. Bustard, V. M. Acosta, J. Nunn, and B. J. Sussman, *J. Mod. Opt.* **63**, 2005 (2016).
- [18] T. van Leent, M. Bock, R. Garthoff, K. Redeker, W. Zhang, T. Bauer, W. Rosenfeld, C. Becher, and H. Weinfurter, *Phys. Rev. Lett.* **124**, 010510 (2020).
- [19] H. P. Specht, C. N olleke, A. Reiserer, M. Uphoff, E. Figueroa, S. Ritter, and G. Rempe, *Nature (London)* **473**, 190 (2011).
- [20] M. K orber, O. Morin, S. Langenfeld, A. Neuzner, S. Ritter, and G. Rempe, *Nat. Photon.* **12**, 18 (2018).
- [21] D.-S. Ding, Z.-Y. Zhou, B.-S. Shi, and G.-C. Guo, *Nat. Commun.* **4**, 2527 (2013).
- [22] Z.-Y. Zhou, Y. Li, D.-S. Ding, W. Zhang, S. Shi, B.-S. Shi, and G.-C. Guo, *Light: Sci. Appl.* **5**, e16019 (2016).
- [23] Z.-Y. Zhou, S.-L. Liu, Y. Li, D.-S. Ding, W. Zhang, S. Shi, M.-X. Dong, B.-S. Shi, and G.-C. Guo, *Phys. Rev. Lett.* **117**, 103601 (2016).
- [24] A. Nicolas, L. Veissier, L. Giner, E. Giacobino, D. Maxein, and J. Laurat, *Nat. Photon.* **8**, 234 (2014).
- [25] Y. Pu, N. Jiang, W. Chang, H. Yang, C. Li, and L. Duan, *Nat. Commun.* **8**, 15359 (2017).
- [26] M. Krenn, M. Huber, R. Fickler, R. Lapkiewicz, S. Ramelow, and A. Zeilinger, *Proc. Natl. Acad. Sci. USA* **111**, 6243 (2014).
- [27] V. Parigi, V. D'Ambrosio, C. Arnold, L. Marrucci, F. Sciarrino, and J. Laurat, *Nat. Commun.* **6**, 7706 (2015).
- [28] D.-S. Ding, W. Zhang, Z.-Y. Zhou, S. Shi, G.-Y. Xiang, X.-S. Wang, Y.-K. Jiang, B.-S. Shi, and G.-C. Guo, *Phys. Rev. Lett.* **114**, 050502 (2015).
- [29] R. Pugatch, M. Shuker, O. Firstenberg, A. Ron, and N. Davidson, *Phys. Rev. Lett.* **98**, 203601 (2007).
- [30] O. Firstenberg, P. London, M. Shuker, A. Ron, and N. Davidson, *Nat. Phys.* **5**, 665 (2009).
- [31] L. Zhao, T. Wang, Y. Xiao, and S. F. Yelin, *Phys. Rev. A* **77**, 041802(R) (2008).
- [32] P. K. Vudyasetu, R. M. Camacho, and J. C. Howell, *Phys. Rev. Lett.* **100**, 123903 (2008).
- [33] M. Shuker, O. Firstenberg, R. Pugatch, A. Ron, and N. Davidson, *Phys. Rev. Lett.* **100**, 223601 (2008).
- [34] Y.-W. Cho, J.-E. Oh, and Y.-H. Kim, *Phys. Rev. A* **86**, 013844 (2012).
- [35] S. Jenkins, D. Matsukevich, T. Chaneliere, A. Kuzmich, and T. Kennedy, *Phys. Rev. A* **73**, 021803(R) (2006).
- [36] D. N. Matsukevich, T. Chaneliere, S. D. Jenkins, S.-Y. Lan, T. A. B. Kennedy, and A. Kuzmich, *Phys. Rev. Lett.* **96**, 033601 (2006).
- [37] L. Li, J. Ji, W. Ren, X. Zhao, X. Peng, J. Xiang, D. L u, and L. Liu, *Chin. Phys. B* **25**, 073201 (2016).
- [38] S.-K. Lee and M. Romalis, *J. Appl. Phys.* **103**, 084904 (2008).
- [39] J. W. Goodman, *Introduction to Fourier Optics* (Roberts and Company Publishers, Colorado, US, 2005), Chap. 5, pp. 97–108.
- [40] P. Tremblay and C. Jacques, *Phys. Rev. A* **41**, 4989 (1990).
- [41] Y.-X. Duan, B. Wang, J.-F. Xiang, Q. Liu, Q.-Z. Qu, D.-S. L u, and L. Liu, *Chin. Phys. Lett.* **34**, 073201 (2017).
- [42] D. A. Steck, "Rubidium 85 d line data," <https://steck.us/alkalidata/rubidium85numbers.pdf>.

- [43] B. Wang, Y. Han, J. Xiao, X. Yang, C. Xie, H. Wang, and M. Xiao, *Opt. Lett.* **31**, 3647 (2006).
- [44] M. Fleischhauer, A. Imamoglu, and J. P. Marangos, *Rev. Mod. Phys.* **77**, 633 (2005).
- [45] M. Fleischhauer and M. D. Lukin, *Phys. Rev. Lett.* **84**, 5094 (2000).
- [46] M. Fleischhauer and M. D. Lukin, *Phys. Rev. A* **65**, 022314 (2002).
- [47] C. Liu, Z. Dutton, C. H. Behroozi, and L. V. Hau, *Nature (London)* **409**, 490 (2001).
- [48] D.-S. Ding, J.-H. Wu, Z.-Y. Zhou, Y. Liu, B.-S. Shi, X.-B. Zou, and G.-C. Guo, *Phys. Rev. A* **87**, 013835 (2013).
- [49] D.-S. Ding, J.-H. Wu, Z.-Y. Zhou, B.-S. Shi, X.-B. Zou, and G.-C. Guo, *Phys. Rev. A* **87**, 053830 (2013).
- [50] D. J. Whiting, N. Šibalić, J. Keaveney, C. S. Adams, and I. G. Hughes, *Phys. Rev. Lett.* **118**, 253601 (2017).
- [51] R. Finkelstein, O. Lahad, I. Cohen, O. Davidson, S. Kiriati, E. Poem, and O. Firstenberg, *Phys. Rev. X* **11**, 011008 (2021).
- [52] L. Viola and S. Lloyd, *Phys. Rev. A* **58**, 2733 (1998).
- [53] M. J. Biercuk, H. Uys, A. P. VanDevender, N. Shiga, W. M. Itano, and J. J. Bollinger, *Nature (London)* **458**, 996 (2009).